BIOCHEMISTRY
including biophysical chemistry & molecular biology

Article

pubs.acs.org/biochemistry

A Role for Catalase-Peroxidase Large Loop 2 Revealed by Deletion Mutagenesis: Control of Active Site Water and Ferric Enzyme Reactivity

Shalley N. Kudalkar,[†] Olive J. Njuma, Yongjiang Li,[‡] Michelle Muldowney, N. Rene Fuanta, and Douglas C. Goodwin*

Department of Chemistry and Biochemistry, Auburn University, Auburn, Alabama 36849-5312, United States

Supporting Information

ABSTRACT: Catalase-peroxidases (KatGs), the only catalase-active members of their superfamily, all possess a 35-residue interhelical loop called large loop 2 (LL2). It is essential for catalase activity, but little is known about its contribution to KatG function. LL2 shows weak sequence conservation; however, its length is nearly identical across KatGs, and its apex invariably makes contact with the KatG-unique C-terminal domain. We used site-directed and deletion mutagenesis to interrogate the role of LL2 and its interaction with the C-terminal domain in KatG structure and catalysis. Single and double substitutions of the LL2 apex had little impact on the active site heme [by magnetic circular dichroism or electron paramagnetic resonance (EPR)] and activity (catalase or peroxidase). Conversely, deletion of a single amino acid from the LL2 apex reduced catalase activity by 80%. Deletion of two or more apex amino acids or all of LL2 diminished catalase activity by 300-fold. Peroxide-dependent but not electron donor-dependent k_{cat}/K_M values for deletion variant peroxidase activity were reduced 20−200-fold, and k_{on} for cyanide binding diminished by 3 orders of magnitude. EPR spectra for deletion variants were all consistent with an increase in the level of pentacoordinate high-spin heme at the expense of hexacoordinate high-spin states. Together, these data suggest a shift in the distribution of active site waters, altering the reactivity of the ferric state, toward, among other things, compound I formation. These results identify the importance of LL2 length conservation for maintaining an intersubunit interaction that is essential for an active site water distribution that facilitates KatG catalytic activity.

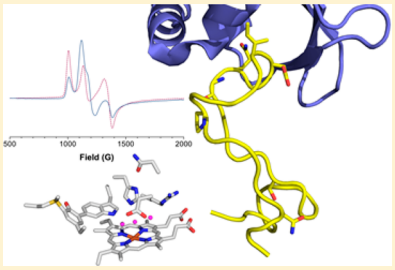

Catalase-peroxidase (KatG) is a heme-dependent enzyme found in bacteria, archaebacteria, fungi, and other lower eukaryotes.[1] KatG from *Mycobacterium tuberculosis* activates the antitubercular prodrug isoniazid. For a large majority of isoniazid-resistant *M. tuberculosis* strains, mutations to the *katG* gene have been identified, the most prominent of which are those that produce S315T KatG.[2] Additionally, KatGs, especially extracellular/periplasmic forms, have been connected with virulence of other pathogens (animal and plant), including *Escherichia coli* O157:H7,[3,4] *Legionella pneumophila*,[5] *Yersinia pestis*,[6,7] and *Magnaporthe* sp.[8−11] Finally, KatGs are a compelling system for investigating heme-dependent enzyme structure and function.[2]

The efficiency of KatG catalase activity rivals that of the monofunctional catalases.[12,13] However, apart from the utilization of a heme prosthetic group, KatG bears no resemblance to these enzymes. The peroxidase activity of KatG is comparable to that of other non-animal peroxidases (now called the peroxidase-catalase superfamily).[1] Sequential and structural analyses place KatG squarely within this superfamily, specifically the class I subdivision along with cytochrome *c* peroxidase (CcP) and the hybrid peroxidase from *Leishmania major*. Strikingly, though the active sites of these enzymes are essentially superimposable, KatG is the lone representative of the superfamily with significant catalase activity.[1,14−18]

The catalytic cycles of typical catalases, typical peroxidases, and a recently proposed mechanism for KatG *catalatic* turnover all begin with the conversion of Fe^{III} heme to Fe^{IV}═O[porphyrin]$^{•+}$ (i.e., compound I) by way of a Fe^{III}−OOH complex known as compound 0 (Scheme 1).[19] The structure of the two-electron-oxidized state varies; in some enzymes, the porphyrin radical is reduced at the expense of the protein as in Fe^{IV}═O[Trp_{191}]$^{•+}$ of CcP.[20,21] The Fe^{III} state of typical catalases returns by the oxidation of H_2O_2 by compound I to generate O_2 and a second equivalent of H_2O. In contrast, the typical peroxidase reaction sequence returns the Fe^{III} state by two sequential one-electron reductions at the expense of an exogenous electron donor.

Though the similarities are remarkable, KatGs have at least four structures, largely peripheral to the active site, that are absent from the other peroxidases, even the hybrid peroxidase from *L. major*.[15,18,22−25] First, there is a gene-duplicated C-terminal domain.[24] Though separated from the active site by ≥30 Å, it appears to help maintain the heme environment for activity by preventing the active site's distal histidine from coordinating the heme iron.[26−28] Second, KatG has three

Received: September 26, 2014
Revised: February 11, 2015
Published: February 12, 2015

DOI: 10.1021/bi501221a
Biochemistry 2015, 54, 1648−1662

Scheme 1. Intermediates of Catalatic and Peroxidatic Turnover[a]

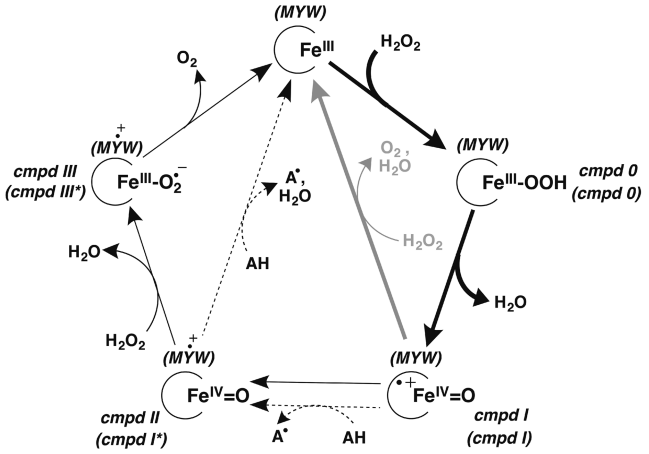

[a]The reactions common to typical non-animal peroxidases, KatG, and typical catalases are shown in bold. The typical peroxidatic cycle also includes the reactions represented by dashed arrows, where AH and A• represent a generic exogenous electron donor and its free radical oxidation product, respectively. A proposed mechanism for KatG catalatic turnover includes reactions represented by bold and solid arrows. The covalent adduct (MYW) and its radical (MYW•+) are unique to KatG as are the designations cmpd I* and cmpd III*. The catalatic reaction sequence for typical catalases is represented by reactions with bold and gray arrows.

interhelical connecting structures with extensions that make them considerably longer than the corresponding structures of other peroxidases. These extensions or large loops are found between helices D and E [i.e., large loop 1 (LL1)], helices F and G [large loop 2 (LL2)], and helices G and H [large loop 3 (LL3)].

A role for LL3 has not been investigated and will not be addressed further here. Conversely, the function of LL1 is the most clearly understood of the three. LL1 bears the strictly conserved tyrosine (Y226 by *E. coli* KatG numbering) that participates in a unique MYW covalent adduct found on the distal side of the heme.[8,18,22,23,29−32] Replacement of any of the members of the adduct invariably eliminates catalase activity without appreciably diminishing the peroxidatic capabilities of the enzyme.[30,32−39] Intramolecular electron transfer follows formation of KatG compound I, producing an Fe^{IV}═O[MYW]$^{•+}$ intermediate termed compound I*. A reaction between compound I* and H_2O_2 is proposed to form an Fe^{III}−$O_2^{•−}$[MYW]$^{•+}$ intermediate (i.e., compound III*). Deprotonation of the adduct Trp followed by formation of an Fe^{III}−OO−Trp(MYW) intermediate has been proposed for this reaction.[40] Finally, electron transfer from the Fe^{III}−$O_2^{•−}$ heme center to the MYW adduct radical produces O_2 and Fe^{III} KatG (Scheme 1).[40−45]

LL1 also bears a strictly conserved glutamate (E253 in *Synechocystis* KatG) that appears at the entrance of a narrow channel to the active site heme. Mutagenesis and computational studies suggest that this residue maintains an ordered orientation of water dipoles that supports H_2O_2 oxidation by KatG.[46,47] Finally, variants that delete the C-terminal end of LL1 not only eliminate catalase activity as expected but also produce substantial gains in peroxidatic activity even over other catalase-negative variants (e.g., Y226F), indicating that LL1 may favor catalase over peroxidase activity by also restricting access of electron donors to the heme edge.[36]

Little is known about the function of LL2, but its presence in all KatGs suggests that it is important. Structures of KatGs show that LL2 begins and terminates adjacent to the active site.[18,22,23,48] Like LL1, portions of LL2 contribute to the narrow active site access channel for H_2O_2. From its point of origin and termination, LL2 extends to make contact with the C-terminal domain of the adjacent subunit (Figure 1). To date,

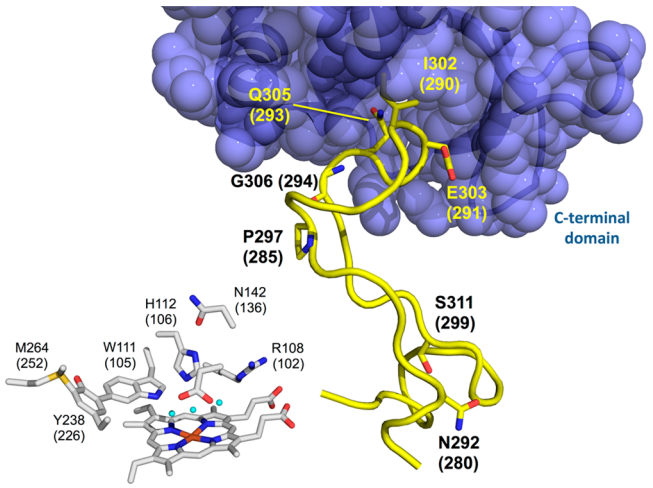

Figure 1. Position of large loop 2 (LL2) relative to the KatG active site and the C-terminal domain. Critical residues found on the distal side of the heme are shown as sticks with carbons colored gray. The α-carbon trace of LL2 is colored yellow with key residues shown as sticks. The portion of the C-terminal domain with which LL2 interacts is shown in blue space-filling format. Coordinates are from Protein Data Bank entry 1MWV.[22] Thus, residue numbering is according to *Burkholderia pseudomallei* KatG with corresponding *E. coli* KatG numbers in parentheses. The image was created using PyMOL.[83]

only two variants targeting LL2 have been evaluated. The *M. tuberculosis* KatG variant W300G, though it forms the MYW adduct, lacks catalase activity but retains *tert*-butyl-OOH-dependent peroxidase activity.[49] Additionally, the entire LL2 structure has been deleted from *E. coli* KatG, producing a 200-fold decrease in catalase activity, but only limited reduction in peroxidase activity.[50] Clearly, the structure is integral to KatG function. However, the manner in which it contributes is unknown. Given that both LL2 and the C-terminal domain are essential to KatG function[26−28,50] and all KatG structures show contact between them, we generated a series of substitution and deletion variants to evaluate this interaction and its impact on the catalytic and spectroscopic properties of KatG.

MATERIALS AND METHODS

Reagents. Oligonucelotide primers were obtained from Invitrogen (Carlsbad, CA). Competent *E. coli* cells (XL-1 Blue and BL-21[DE3]pLysS) and *Pfu* polymerase were from Agilent Technologies (La Jolla, CA). Restriction enzymes were from New England Biolabs (Beverly, MA). QIAprep Spin Miniprep kits and nickel-nitriloacetic acid (Ni-NTA) resin were obtained from Qiagen (Valencia, CA). Isopropyl β-D-thiogalactopyranoside (IPTG) was obtained from Gold Biotechnology Inc. (St. Louis, MO). Mono- and dibasic sodium phosphate, acetic acid, and sodium acetate were from Fisher (Pittsburgh, PA). Bugbuster and benzonase nuclease were from EMD (Madison,

DOI: 10.1021/bi501221a
Biochemistry 2015, 54, 1648−1662

WI). Ampicillin, chloramphenicol, imidazole, hemin, sodium dithionite, 2,2′-azinobis(3-ethylbenzothiazoline-6-sulfonic acid) (ABTS), and hydrogen peroxide (30%) were all from Sigma (St. Louis, MO). Water purified through a Barnstead EasyPure II system (18.2 MΩ/cm resistivity) was used to make all buffers and media.

Amino Acid Sequence Alignments. KatG sequences were selected to maximize diversity[1] and to include some of the most intensely investigated enzymes. Sequence alignments were performed with ClustalX 2.1 using the Gonnet protein weight matrix. The gap-opening penalty was set to 8, and the gap-extension penalty was set to 0.2. Abbreviations correspond to those used by Zamocky et al.[1] Except where noted, sequences were obtained under the following UniProt accession numbers: *M. tuberculosis* KatG (MtuKatG), P9WIE5; *E. coli* O157:H7 KatP (EcoKatP), Q7BSW8; *Le. pneumophila* KatG2 (LpnKatG2), Q5ZZ17; *Haloarcula marismortui* (HmaKatG1), Q5 V0S5; *Rhodopirellula baltica* KatG (RbaKatG), Q7UUW9; *Bu. pseudomallei* KatG (BpKatG), Q939D2; *Comamonas terrigena* KatG (CterKatG1), C0JSV4; *Burkholderia xenovorans* KatG (BxKatG1), Q13US7; *E. coli* KatG (EcoHPI), P13029; *Pseudomonas fluorescens* (PfKatG1), Q4KD86; *Flavobacterium Johnsoniae* (FjKatG), A5FD11; *Magnaporthe grisea* KatG1 (MagKatG1), A4R5S9; *M. grisea* KatG2 (MagKatG2), A4QUT2; *Aspergillus niger* KatG1 (AnKatG1), A2Q7T1; *Penicillium marneffei* KatG1 (PmKatG1), Q8NJN2; *Neurospora crassa* KatG (NcKatG1), Q8X182; *Geobacillus stearothermophilus* (GstKatG1), P14412; *Synechocystis* PCC6803 KatG (SYspKatG1), P73911; *Acidovorax avenae* KatG1 (AavKatG1), A1TRV8; *Methanosarcina acetivorans* KatG (MacKatG1), Q8TS34; *Ralstonia solanacearum* KatG (RsoKatG1), GenBank locus CBJ43830.

Site-Directed and Deletion Mutagenesis. Plasmids for expression of KatG LL2 substitution and deletion variants were generated from our pET20b-based construct for the expression of *E. coli* KatG using the polymerase chain reaction-based "around-the-horn" approach.[51] Table S1 of the Supporting Information lists the mutagenic primers used in this study and the diagnostic restriction digest used for candidate plasmid screening. Amplification products through ligation and screening were handled as previously described.[28] Positive candidates were sent for full DNA sequence analysis (Davis Sequencing, Inc., Davis, CA) to confirm that the correct modifications had been introduced without any unintended mutations into the *katG* gene.

Expression and Purification of KatG Variants. Protein expression was conducted in Luria-Bertani broth supplemented with ampicillin (0.1 mg/mL) and chloramphenicol (0.034 mg/mL) as previously described,[52] except that cultures were not supplemented with δ-aminolevulinic acid or ferrous ammonium sulfate. Protein purification was based on Ni-NTA affinity and was conducted as previously described[50] with the following additions. An initial wash step with 50 mM Tris buffer (pH 8.0) was performed to remove phosphate-precipitating ions. The column was then washed with 50 mM phosphate (pH 8.0) and 200 mM NaCl (buffer A). Subsequent washes were performed using buffer A supplemented with 2 mM imidazole and then 20 mM imidazole. KatG and its LL2 variants were then eluted using buffer A supplemented with 50 mM and/or 200 mM imidazole. Excess imidazole was removed by gel filtration chromatography using 10DG columns (Bio-Rad, Hercules, CA) equilibrated with 50 mM phosphate (pH 7.0) and 50 mM NaCl. The concentration of purified enzyme was determined by the method of Gill and Von Hippel[53] using an ε_{280} of 1.44 × 10^5 M^{-1} cm^{-1} for all the variants with the exception of KatG (ΔLL2) and W297F KatG, for which ε_{280} = 1.37 × 10^5 M^{-1} cm^{-1}.

Enzyme Reconstitution, UV−Vis Spectroscopy, Size-Exclusion Chromatography, and MYW Sodium Dodecyl Sulfate−Polyacrylamide Gel Electrophoresis (SDS−PAGE). Wild-type KatG and its variants were reconstituted with 0.9 equiv of hemin. Following a 24 h incubation at 4 °C, each reconstituted protein was centrifuged (16100*g* for 5 min) to remove any free hemin or insoluble protein. All UV−visible absorption spectra (800−250 nm) were recorded at room temperature in 0.2 M phosphate buffer (pH 7.0) using a Shimadzu UV-1601 spectrophotometer. The holoprotein concentration was determined according to the method of Falk.[54]

Evaluation of the quaternary structure of wild-type KatG and selected variants was conducted using an Agilent Technologies (Santa Clara, CA) 1260 Infinity high-performance liquid chromatography (HPLC) instrument equipped with a 7.8 mm × 300 mm Bio SEC-3 size-exclusion column (range of 0.005−1.5 MDa). An isocratic mobile phase of 5.0 mM phosphate (pH 7.0) was used at a flow rate of 1.00 mL/min. Separations were conducted at 4 °C, and elution was monitored at 280 and 400 nm by a diode array detector.

SDS−PAGE was used to evaluate MYW covalent adduct formation by KatG and selected variants. Briefly, heme-reconstituted proteins were incubated with peroxide (20 equiv of H_2O_2, 10 equiv of *tert*-butyl-OOH, or 10 equiv of *m*-chloroperoxybenzoic acid) for 10 min. Following incubation, each protein was denatured, loaded, and electrophoresed by SDS−PAGE (7.6% acrylamide) alongside the corresponding apoprotein and holoprotein unreacted with peroxide. To illustrate, gels comparing results for wild-type and ΔLL2 KatG are shown in Figures S1 and S2 of the Supporting Information.

Circular Dichroism Spectropolarimetry (CD). Far-UV CD spectra were recorded for all variants prior to reconstitution with hemin. Each protein (5 μM) was placed in 5 mM phosphate (pH 7.0). All spectra were recorded using a 0.05 cm quartz cell in a Jasco (Oklahoma City, OK) J-180 spectropolarimeter. All spectra were collected using the following settings: λ range of 180−300 nm, data pitch of 0.05 nm, scan speed of 50 nm/min, and eight scans accumulated. Baseline corrections and data analyses were conducted using Jasco J-720 software.

Magnetic Circular Dichroism (MCD) Spectroscopy. The J-180 spectropolarimeter equipped with a 1.4 T permanent magnet cell holder was used. Target protein (15 μM) was placed in 50 mM phosphate (pH 7.0) and 50 mM NaCl. Spectra were recorded using a 0.5 cm quartz cell. All ferric spectra were recorded at room temperature using the following settings: λ range of 700−350 nm, continuous scan mode, scan speed of 50 nm/min, data pitch of 0.1 nm, and eight scans accumulated. For ferrous MCD spectra, a small amount (i.e., <1 mg) of sodium dithionite was added to the sample cuvette and mixed. For spectra of ferrous states, all scan settings were the same except that only four repetitive scans were accumulated. In all cases, spectra were recorded with and without a magnetic field, and the former was subtracted from the latter to obtain the MCD spectrum. A spectrum recorded for buffer alone was used for baseline subtraction. Baseline corrections and data analyses were conducted using Jasco J-720 software.

DOI: 10.1021/bi501221a
Biochemistry 2015, 54, 1648−1662

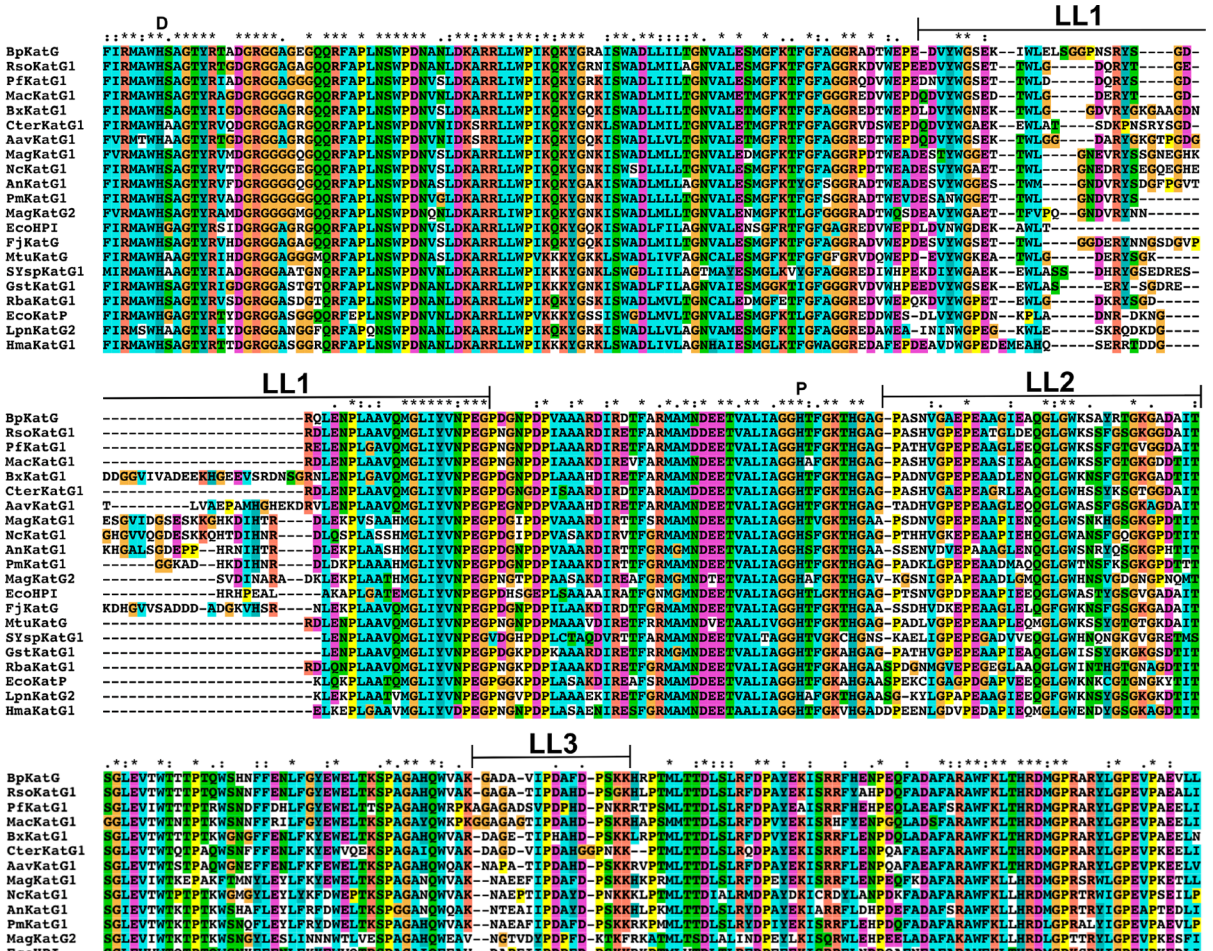

Figure 2. Amino acid sequence alignments for multiple KatGs. Sequence alignments were performed using the entire amino acid sequence for each protein, but only residues equivalent to BpKatG F106−L445 (EcKatG F100−I433) are shown. The relative positions of LL1−LL3 are indicated as are the active site distal histidine (D) and proximal histidine (P) ligand to the heme iron.

Electron Paramagnetic Resonance Spectroscopy. EPR spectra were recorded using a Bruker EMX instrument equipped with an Oxford ESR 900 cryostat and ITC temperature controller. Wild-type KatG and its LL2 variants were concentrated to ∼150 μM using Amicon Ultra-4 centrifuge filter devices (MW cutoff of 50 kDa). Spectrometer settings were as follows: temperature, 10 K; center field, 3250 G; sweep width, 5500 G; receiver gain, 1.0×10^5; microwave power, 9.38 GHz; modulation amplitude, 10 G; modulation frequency, 100 kHz; time constant, 655.36 ms; conversion time, 655.36 ms. Spectral simulation and spin quantification were performed using the Biomolecular EPR Spectroscopy Software package available online.[55,56]

Catalase and Peroxidase Activity Assays. Catalase activity was evaluated by monitoring the decrease in H_2O_2 concentration at 240 nm (ε_{240} = 39.4 M^{-1} cm^{-1}).[57] All assays contained 10 nM enzyme in 100 mM phosphate (pH 7.0) and were conducted at room temperature using a Shimadzu UV-1601 spectrophotometer. Peroxidase activity was measured by monitoring the production of ABTS radical at 417 nm (ε_{417} = 34.7 mM^{-1} cm^{-1})[58] in the presence of H_2O_2 or *tert*-butyl-OOH. Concentrations of ABTS in stock solutions were determined spectrophotometrically (ε_{340} = 3.66×10^4 M^{-1} cm^{-1}).[58] All peroxidase assays using H_2O_2 contained 10 nM enzyme, and all assays using *tert*-butyl-OOH contained 50 nM enzyme. All assays were conducted at room temperature using 50 mM acetate (pH 5.0) and were initiated by the addition of peroxide.

For catalase and peroxidase activities, we typically observed a hyperbolic dependence of rate on substrate concentration. Thus, the data were fit to a standard Michaelis−Menten function (eq 1) to obtain the *apparent* kinetic parameters, k_{cat}, K_M, and k_{cat}/K_M.

$$\frac{v_0}{[E]_T} = \frac{k_{cat}[S]}{K_M + [S]} \quad (1)$$

These are termed *apparent* parameters because they cannot be assigned the physical interpretation usually connected with the Michaelis−Menten model. Thus, k_{cat}, as it is applied here, is the asymptotic maximum $v_0/[E]_T$ approached as substrate concentration increases; the apparent K_M is the substrate concentration necessary to produce a $v_0/[E]_T$ equal to $1/2k_{cat}$, and k_{cat}/K_M is the rate response observed at low concentrations

DOI: 10.1021/bi501221a
Biochemistry 2015, 54, 1648−1662

Table 1. Apparent Kinetic Parameters for Catalase Activity of KatG LL2 Variants[a]

	KatG	k_{cat} (s^{-1})	K_M (mM)	k_{cat}/K_M ($\times 10^6$ M^{-1} s^{-1})	fraction k_{cat}
group I	wild-type	12000 ± 1000	3.7 ± 0.3	3.3 ± 0.1	1.00
	I290V	8000 ± 200	3.9 ± 0.3	3.7 ± 0.3	0.67
	Q293V	5300 ± 500	3.1 ± 0.5	1.7 ± 0.1	0.44
	I290V/Q293V	5600 ± 400	3.2 ± 0.4	1.8 ± 0.1	0.47
	I290A	10300 ± 600	4.0 ± 0.7	2.6 ± 0.3	0.93
	Q293A	12200 ± 1400	4.6 ± 0.8	2.7 ± 0.2	1.02
	I290A/Q293A	7700 ± 1100	4.2 ± 0.9	1.8 ± 0.2	0.64
	Q293E	9600 ± 700	8 ± 1	1.3 ± 0.1	0.80
	E291A	16700 ± 300	5.9 ± 0.2	2.8 ± 0.1	1.39
	E291K	9500 ± 200	2.1 ± 0.1	4.5 ± 0.4	0.79
	E291K/E292A	12200 ± 300	2.5 ± 0.1	4.8 ± 0.1	1.02
group II	IEEQ-A	630 ± 70	3.7 ± 1.5	0.19 ± 0.05	0.053
	ΔN280/ΔS299	2500 ± 100	3.3 ± 0.5	0.79 ± 0.09	0.21
	ΔP285/ΔG294	1770 ± 80	2.2 ± 0.2	0.80 ± 0.03	0.15
	Δ291	2000 ± 100	3.1 ± 0.1	0.65 ± 0.03	0.18
group III	Δ291−292	N/D[b]	N/D[b]	N/D[b]	N/D[b]
	Δ290−293	37 ± 6	5 ± 1	0.0074 ± 0.0005	0.0031
	Δ288−293	N/D[b]	N/D[b]	N/D[b]	N/D[b]
	ΔLL2	N/D[b]	N/D[b]	N/D[b]	N/D[b]

[a]All assays were conducted using 100 mM phosphate buffer (pH 7.0) at 23 °C. [b]Not determined.

of the varied substrate and a measure of relative efficiency. It is possible to obtain the latter values even if it is not practical to reach saturating concentrations of one or both substrates. Further, where there is little or no catalase activity, the peroxidase k_{cat}/K_M with respect to peroxide is expected to be twice the second-order rate constant for peroxide-dependent compound I formation. Similarly, the k_{cat}/K_M with respect to ABTS is expected to be twice the second-order rate constant for the rate-determining step in the reduction of the enzyme back to its ferric state (see the Supporting Information for additional explanation).

On rare occasions, weak substrate-dependent inhibition was observed. To ensure that the apparent kinetic parameters were undistorted by the inhibition effect, we applied eq 2. This equation includes an *apparent* dissociation constant (K_I) corresponding to the substrate's action as an inhibitor.

$$\frac{v_o}{[E]_T} = \frac{k_{cat}[S]}{K_M + [S] + [S]^2/K_I} \quad (2)$$

Here, K_I is a macroscopic parameter that accounts for the inhibitory effect. In each case, where any inhibition was observed, the apparent K_I was 30−100-fold greater than the apparent K_M, confirming the relatively small contribution of substrate-dependent inhibition.

Cyanide Binding Studies. Cyanide binding was evaluated by equilibrium titration and stopped flow. Titrations were monitored using a Shimadzu UV-1601 spectrophotometer. These were performed by adding 1−2 μL aliquots of a KCN stock solution to 1 mL of each variant (1 μM). After each portion of cyanide was added, the solution was thoroughly mixed, and the optical spectrum was recorded after 3 min to ensure completion of the binding reaction. The change in absorbance at 422 nm was plotted versus KCN concentration to obtain the dissociation constants. All titrations were conducted at room temperature in 50 mM phosphate (pH 7.0).

Rates of cyanide binding were monitored by stopped flow using a PC-upgraded SX.18MV Rapid Reaction Analyzer (Applied Photophysics, Leatherhead, U.K.) in single-mixing mode. All reactions were conducted at 25 °C in 50 mM phosphate (pH 7.0). The enzyme (6 μM) was held in one syringe, and KCN (0.03−1.0 mM) was held in the second. Full spectra were recorded by a diode array detector, and single-wavelength data were recorded at 428 nm to monitor formation of the Fe^{III}−CN complex. A single-exponential function produced poor fits of reaction curves regardless of the protein being evaluated or the concentration of cyanide used. For the wild type and Q293A, at least a three-exponential function was necessary to produce satisfactory fits of the data, and a two-exponential function was necessary to account for cyanide binding by the IEEQ-A, Δ291, Δ291−292, Δ290−293, Δ288−293, and ΔLL2 variants.

RESULTS

LL1 versus LL2. Sequence alignments for KatGs from across the phylogenetic spectrum (Figure 2) illustrate striking differences between the three KatG-unique interhelical insertions (LL1−LL3). Sequences for 21 KatGs were taken such that all three of the major clades identified by Zamocky et al. were represented.[1] The fungal enzymes selected included intracellular and secreted forms, and prokaryotic representatives were taken from Archaea, Proteobacteria, Bacteroidetes, and Cyanobacteria. The length of LL1 varied considerably (39−70 residues) across the selected subset of enzymes. Further, the N-terminal two-thirds of the structure showed little in the way of sequence conservation, but the C-terminal one-third was nearly invariant across all KatGs. Conversely, LL2 showed almost no variation in its length (35 or 36 amino acids), but substantial variation in sequence. Of only five strictly conserved residues in LL2, three were glycines and a fourth was proline. These residues are more frequently important for their ability to fulfill specific conformational constraints rather than for particular noncovalent interactions with other residues. The fifth strictly conserved residue was a Trp (W297 in *E. coli* KatG). We expressed, purified, and characterized W297F KatG, but it showed catalytic properties (catalase and peroxidase) essentially identical to those of the wild type (data not shown).

KatG LL2 Variants. Two LL2 residues are prominent in the interaction between LL2 and the C-terminal domain. By *E. coli*

DOI: 10.1021/bi501221a
Biochemistry 2015, 54, 1648−1662

Table 2. Apparent Kinetic Parameters for Peroxidase Activity with Respect to H_2O_2[a]

	KatG	k_{cat} (s^{-1})	K_M (mM)	k_{cat}/K_M ($\times 10^5$ M^{-1} s^{-1})	fraction k_{cat}/K_M
group I	wild-type[a]	83 ± 2	0.31 ± 0.05	2.7 ± 0.1	1.00
	I290V	26 ± 3	0.08 ± 0.01	3.5 ± 0.1	1.30
	Q293V	26 ± 2	0.5 ± 0.1	0.49 ± 0.04	0.18
	I290V/Q293V	24 ± 2	0.21 ± 0.04	1.1 ± 0.1	0.41
	I290A	26 ± 1	0.09 ± 0.01	3.1 ± 0.3	1.15
	Q293A	27.8 ± 0.2	0.078 ± 0.004	3.8 ± 0.4	1.41
	I290A/Q293A	13.6 ± 0.7	0.07 ± 0.02	2.1 ± 0.6	0.78
	Q293E	23.8 ± 0.4	0.089 ± 0.001	2.68 ± 0.03	0.99
	E291A	40 ± 2	0.10 ± 0.01	3.9 ± 0.1	1.44
	E291K	34 ± 2	0.06 ± 0.01	6 ± 1	2.22
	E291K/E292A	35.3 ± 0.3	0.06 ± 0.01	6.2 ± 0.1	2.30
group II	IEEQ-A	99 ± 11 (39)[b]	75 ± 18	0.013 ± 0.002	0.0048
	ΔN280/ΔS299	224 ± 46 (104)	58 ± 17	0.039 ± 0.004	0.014
	ΔP285/ΔG294	332 ± 178 (66)	199 ± 122	0.018 ± 0.003	0.0067
	Δ291	184 ± 9 (100)	41 ± 3	0.046 ± 0.001	0.017
group III	Δ291−292	273 ± 49 (88)	107 ± 38	0.027 ± 0.005	0.01
	Δ290−293	684 ± 578 (80)	366 ± 329	0.020 ± 0.002	0.0074
	Δ288−293	85 ± 12	13 ± 3	0.065 ± 0.005	0.024
	ΔLL2	27.9 ± 0.9	2.2 ± 0.2	0.12 ± 0.01	0.044

[a]All assays were conducted using 0.5 mM ABTS and 50 mM acetate buffer (pH 5.0) at 23 °C. [b]Because saturating concentrations of H_2O_2 were not achieved, values in parentheses indicate the largest observed $v_0/[E]_T$ (s^{-1}).

numbering, these are I290 and Q293. Residue 290 is conserved as a hydrophobic side chain (Val, Ile, Leu, or Met), and residue 293 is often a Gln, though hydrophobic side chains like Met are occasionally observed. We evaluated the effect of site-specific substitution of these residues on KatG structure and function, replacing each one and both with Val and Ala. Additionally, we substituted E291 and E292, and a quadruple variant in which all four amino acids (290−293) were each substituted with an alanine (IEEQ-A). Because length appeared to be a conserved feature necessary to make contact with the C-terminal domain, a panel of deletion variants was also generated, eliminating some or all of the apex of LL2: Δ291, Δ291−292, Δ290−293, and Δ288−293. We also shortened LL2 by removing an amino acid from its ascending and descending limbs (i.e., its N-terminal half and C-terminal half, respectively). The first variant achieved this by removing the strictly conserved Pro 285 and Gly 294 (ΔP285/ΔG294), and the second did so by removing two residues that showed much weaker sequence conservation, Asn 280 and Ser 299 (ΔN280/ΔS299). These were compared against the wild-type enzyme and KatG lacking the entire LL2 structure (ΔLL2) generated previously in our laboratory.[50] All the variants were expressed in a soluble state and upon purification showed CD spectra highly similar to that of the wild type,[27] indicating that neither the substitutions nor the deletions resulted in gross misfolding of the variants (data not shown).

Catalatic and Peroxidatic Activities of LL2 Variants. The variants divided into three groups based upon a combined consideration of their reactions involving H_2O_2 (catalase activity and peroxidase activity with respect to H_2O_2 concentration) (Tables 1 and 2, respectively). For catalase k_{cat}, group I variant values ranged from 40 to 140% of that of wild-type KatG. All of the single- and double-substitution variants fell in this category. Group III variants showed a decrease of at least 300-fold in k_{cat} compared to that of the wild-type enzyme. This group included variants with two or more residues deleted from the apex of LL2 (Δ291−292, Δ290−293, and Δ288−293) as well as KatG lacking the entire LL2 structure (ΔLL2). The intermediate group II variants all showed catalase k_{cat} values between 5 and 21% of that of the wild-type enzyme. Included in group II were variants in which (1) residues 290−293 were each substituted with Ala (IEEQ-A), (2) a single residue was deleted from the LL2 apex (i.e., Δ291), and (3) a residue from the ascending and descending limbs of LL2 was deleted (i.e., ΔP285/ΔG294 and ΔN280/ΔS299). Evaluation of k_{cat}/K_M produced comparable results. By an SDS−PAGE-based procedure, group II and III variants appeared to be able to form the MYW covalent adduct in a manner similar to that of the wild-type enzyme, indicating that diminished catalase activity was due to other factors (data not shown).

Variants from all three groups displayed appreciable peroxidase activity, but there was a sharp distinction in the apparent kinetic parameters obtained for group I on one hand versus groups II and III on the other. With respect to H_2O_2 concentration, group I variants were largely similar to the wild-type enzyme (Table 2). For group II and III variants, rates of peroxidase activity were similar to that of wild-type KatG, but far higher concentrations of H_2O_2 were required to obtain them. Consequently, the most reliable parameters for comparison were the k_{cat}/K_M with respect to H_2O_2 and the electron donor. Accordingly, the group II and III variants showed markedly decreased peroxidatic efficiency with respect to H_2O_2 (Table 2). In light of the lack of interfering catalase activity in the group III variants in particular, the low k_{cat}/K_M values with respect to H_2O_2 are indicative of slow rates of compound I formation. Indeed, when the peroxidase activities of group II and III variants were evaluated with *tert*-butyl-OOH in place of H_2O_2, k_{cat}/K_M values with respect to this peroxide were diminished 25−100-fold compared to that of the wild-type enzyme. With respect to the electron donor (ABTS), all three variant groups produced kinetic parameters similar to those of the wild-type enzyme; however, generally group I variants showed lower k_{cat}/K_M values with respect to ABTS, while group II and especially group III variants produced k_{cat}/K_M values greater than that of the wild-type enzyme (Table 3).

DOI: 10.1021/bi501221a
Biochemistry 2015, 54, 1648−1662

Table 3. Apparent Kinetic Parameters for Peroxidase Activity with Respect to ABTS[a]

	KatG	k_{cat} (s^{-1})	K_M (mM)	k_{cat}/K_M ($\times 10^5$ M^{-1} s^{-1})	fraction k_{cat}/K_M
group I[b]	wild-type	55 ± 1	0.087 ± 0.008	6.3 ± 0.1	1.00
	I290V	28.5 ± 0.8	0.13 ± 0.01	2.2 ± 0.2	0.35
	Q293V	15.2 ± 0.5	0.09 ± 0.01	1.6 ± 0.2	0.25
	I290V/Q293V	22.5 ± 0.4	0.081 ± 0.006	2.8 ± 0.2	0.44
	I290A	32.5 ± 0.4	0.16 ± 0.01	2.0 ± 0.1	0.31
	Q293A	29.3 ± 0.2	0.08 ± 0.01	3.7 ± 0.7	0.59
	I290A/Q293A	13.3 ± 0.4	0.037 ± 0.003	3.5 ± 0.2	0.56
	Q293E	20 ± 2	0.05 ± 0.01	3.9 ± 0.9	0.62
	E291A	39.7 ± 0.5	0.071 ± 0.003	5.6 ± 0.2	0.89
	E291K	29.6 ± 0.1	0.023 ± 0.001	12.6 ± 0.9	2.00
	E291K/E292A	38 ± 2	0.028 ± 0.006	14 ± 2	2.22
group II[c]	IEEQ-A	70 ± 1	0.029 ± 0.002	24 ± 2	3.81
	ΔN280/ΔS299	54 ± 2	0.075 ± 0.008	7.3 ± 0.7	1.16
	ΔP285/ΔG294	29 ± 1	0.069 ± 0.008	4.2 ± 0.3	0.67
	Δ291	68.5 ± 0.3	0.062 ± 0.003	11 ± 1	1.75
group III[c]	Δ291−292	54.5 ± 0.1	0.020 ± 0.001	28 ± 2	4.44
	Δ290−293	37.7 ± 0.5	0.022 ± 0.001	16.8 ± 0.7	2.67
	Δ288−293	65.2 ± 0.8	0.041 ± 0.007	16 ± 3	2.54
	ΔLL2	27 ± 3	0.013 ± 0.001	21 ± 1	3.33

[a]All assays were conducted using 50 mM acetate buffer (pH 5.0) at 23 °C. [b]Assays contained 0.5 mM H_2O_2. [c]Assays contained 20 mM H_2O_2.

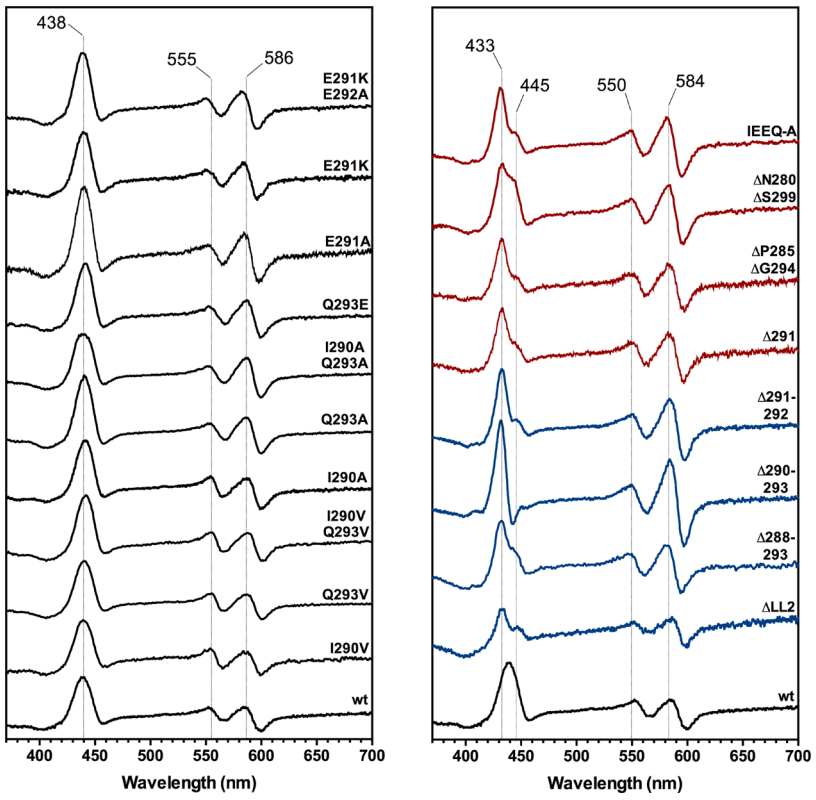

Figure 3. MCD spectra for the ferrous state of LL2 variants. Spectra for single- and double-substitution variants (i.e., group I based on their catalase activity) are compared to that of wild-type KatG in the left panel. Spectra for the deletion variants and IEEQ-A [i.e., groups II (red) and III (blue) based on their catalase activity] are compared to that of wild-type KatG in the right panel. All spectra were recorded in 50 mM phosphate (pH 7.0) and 50 mM NaCl at 23 °C.

Given the intersubunit nature of the interaction between LL2 and the C-terminal domain, the quaternary structure of the group II and III variants was evaluated by size-exclusion chromatography. For the wild type and all group II and III variants, the dominant elution peak corresponded to a MW between 343 kDa (wild type) and 327 kDa (ΔLL2), but in no case were peaks corresponding to a lower MW detected. When we accounted for the subunit molecular weight for each protein, a subunit number between 4.1 and 4.2 was calculated for wild-type KatG and each variant. This was consistent with the previous assignment of cytosolic *E. coli* KatG (i.e., HPI) as a tetrameric enzyme[59] and suggested that the alterations in activity observed for the group II and III variants were not due to changes in the quaternary structure of the enzyme.

DOI: 10.1021/bi501221a
Biochemistry 2015, 54, 1648−1662

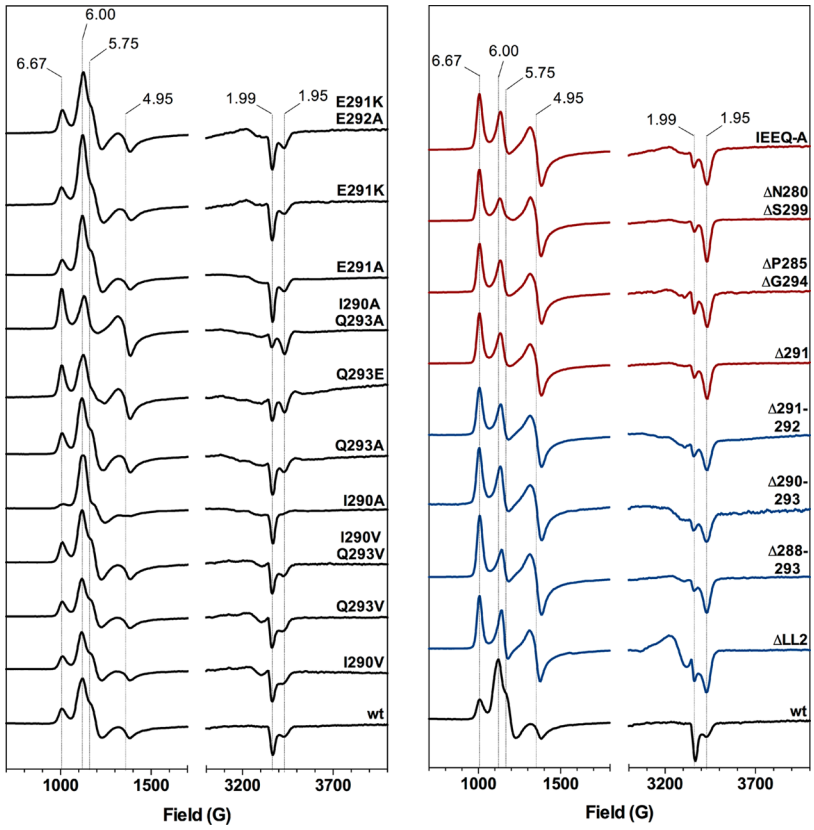

Figure 4. EPR spectra for the ferric state of KatG LL2 variants. Spectra for single- and double-substitution variants (i.e., group I based on their catalase activity) are compared to that of wild-type KatG in the left panel. Spectra for the deletion variants and IEEQ-A [i.e., groups II (red) and III (blue) based on their catalase activity] are compared to that of wild-type KatG in the right panel. Spectrometer settings were as follows: temperature, 10 K; microwave frequency, 9.38 GHz; microwave power, 0.1 mW; modulation amplitude, 10 G; modulation frequency, 100 kHz.

Spectroscopic Properties of LL2 Variants. Magnetic circular dichroism (MCD) spectra for high-spin ferric KatG are consistent with those of other high-spin ferric heme proteins, showing low-intensity features near 410 and 555 nm.[60,61] All of the variants showed ferric MCD spectra very similar to those observed for wild-type KatG (data not shown). The KatG ferrous state shows MCD spectral features much more intense than those of the ferric state, making it a useful probe of active site heme environment. Ferrous MCD spectra for wild-type KatG were also consistent with high-spin heme as the dominant state (i.e., an intense C-type feature at 438 nm and relatively weak bands at 555 and 586 nm).[62] With the exception of a slightly broadened feature at 438 nm for the I290A/Q293A variant, spectra for the group I variants were indistinguishable from that of the wild-type enzyme (Figure 3). However, group II and III variants showed a split feature (433 and 445 nm) rather than the single band at 438 nm. The relative contribution of each feature to the spectrum varied from Δ290−293, which showed only the band at 433 nm, to ΔN280/ΔS299, which showed nearly equal contributions at 433 and 445 nm. Importantly, wild-type KatG and all variants lacked the very intense A-term centered at 550 nm that is typical of hemoproteins bearing low-spin ferrous hemes,[60,61] suggesting that differences between group I and groups II and III were due to the presence of alternative high-spin states.

Accordingly, low-spin states were essentially absent from EPR spectra for ferric wild-type KatG and all the LL2 variants (Figure 4). In all cases, a multiplicity of high-spin states was observed. These states were differentiated from one another on the basis of the **g** tensor anisotropy that was most apparent in the $g \sim 6$ region of the spectrum. Consistent with recent reports on ferric KatG from *M. tuberculosis*,[63] we observed as many as four high-spin contributors to the EPR spectra of our group I variants. The two most easily identifiable were a species with relatively large rhombic distortion ($g_x \sim 6.6$, $g_y \sim 4.95$, and $g_z \sim 1.95$) and a species with relatively small rhombic distortion ($g_x \sim 6.0$, $g_y \sim 5.6$, and $g_z \sim 1.99$). The most satisfactory EPR spectral simulations also included a species exhibiting an intermediate rhombic distortion ($g_x \sim 6.3$, $g_y \sim 5.2$, and $g_z \sim 1.99$) and a small contribution from an axial species ($g_\perp \sim 5.85$, and $g_\parallel \sim 1.99$). EPR spectral simulations revealed that the typical spectrum of a group I variant was similar to that of the wild type, exhibiting contributions of ∼40% from broad rhombic, ∼25% from intermediate rhombic, ∼30% from narrow rhombic, and ∼5% from axial components (Table 4). In contrast, the most satisfactory spectral simulations for group II and III variants included contributions from only three high-spin species; a species with narrow rhombic distortion was virtually absent from the spectra for these variants. Further, the contribution from an intermediate rhombic species was diminished by a factor of ∼2. Finally, the relative contributions from a broad rhombic (75−85%) and an axial (10%) species were roughly twice the intensity of those observed in most of the group I variants (Table 4). Two group I variants, Q293E and I290A/Q293A, showed EPR spectra that were more similar to those of groups II and III. However, in all other respects, Q293E and I290A/Q293A resembled other group I variants.

DOI: 10.1021/bi501221a
Biochemistry 2015, 54, 1648−1662

Table 4. Contribution of Heme States from EPR Spectral Simulation

	KatG	% contribution to EPR spectrum			
		BR[a]	IR[b]	NR[c]	AX[d]
group I	wild-type	38.1	22.2	32.8	6.8
	I290V	39.5	23.3	31.9	5.3
	Q293V	44.0	21.7	29.4	5.6
	I290V/Q290V	42.5	21.7	30.3	5.5
	I290A	14.9	20.1	41.7	23.3
	Q293A	41.3	22.7	30.5	5.53
	I290A/Q293A	78.0	5.1	5.6	11.3
	Q293E	63.2	9.0	13.8	13.9
	E291A	32.5	19.5	41.3	6.5
	E291K	35.1	17.8	47.1	–
	E291K/E292A	38.9	12.8	41.2	7.1
group II	IEEQ-A	77.2	11.3	–	11.4
	ΔN280/ΔS299	76.8	11.8	–	11.4
	ΔP285/ΔG294	77.9	10.4	–	11.7
	Δ291	79.6	9.5	–	10.9
group III	Δ291–292	78.3	10.8	–	10.9
	Δ290–293	81.0	9.1	–	9.9
	Δ288–293	85.6	6.5	–	7.9
	ΔLL2	78.7	9.2	–	12.1

[a]Broad rhombic: $g_x \sim 6.6$, $g_y \sim 4.95$, and $g_z \sim 1.95$. [b]Intermediate rhombic: $g_x \sim 6.3$, $g_y \sim 5.2$, and $g_z \sim 1.99$. [c]Narrow rhombic: $g_x \sim 6.0$, $g_y \sim 5.6$, and $g_z \sim 1.99$. [d]Axial: $g_\perp \sim 5.85$, and $g_\parallel \sim 1.99$.

Cyanide Titrations and Binding Kinetics. The substantially diminished k_{cat}/K_M values with respect to H_2O_2 combined with the unaffected or enhanced k_{cat}/K_M values with respect to the reducing substrate (see Tables 2 and 3) pointed to a compromised ability of the group II and III variants to react with H_2O_2 to form compound I. Attempts to directly monitor the reaction of H_2O_2 with the ferric forms of these enzymes were unsuccessful because of the relatively slow rate of reaction with H_2O_2 combined with subsequent reactions leading to heme bleaching when high concentrations of H_2O_2 were employed. Cyanide binding by ferric peroxidases has several features that correspond to the steps involved in compound I formation, and as such, the former has been used as a mimic of the latter.[19,64,65] We evaluated cyanide binding by wild-type KatG, a representative of the group I variants (Q293A), representatives of the group II variants (IEEQ-A and Δ291), and all the group III variants (Δ291–292, Δ290–293, Δ288–293, and ΔLL2).

Titration of the wild type and variants from all three groups with cyanide showed formation of an Fe^{III}–CN complex (Figure S3 of the Supporting Information). The K_D values obtained for wild-type and Q293A KatG were nearly identical, but those obtained for group II and III variants were elevated 6-fold (Δ291) to 30-fold (Δ290–293), with most increased ∼15-fold (Table 5).

As with titration, the spectral transitions observed by stopped flow were consistent with formation of the Fe^{III}–CN complex for all proteins evaluated. Spectra recorded for Q293A KatG and the IEEQ-A variant are shown in Figure 5. Spectra collected for Δ291 and all the group III variants were indistinguishable from those observed for IEEQ-A (data not shown). Generally, the rates of Fe^{III}–CN complex formation were far more rapid for wild-type and Q293A KatG than for the group II and III variants (Figure 5C). However, for the wild type and all the variants, a single-exponential function produced poor fits of the individual reaction progress curves. At least three exponentials were necessary to account for wild-type and Q293A KatG; a fourth was required if long reaction times (e.g., 100 s) were considered. For the group II and III variants, a two-exponential function was adequate to account for the data even over long reaction times.

Table 5. Dissociation Constants for Cyanide Binding Determined by Equilibrium Titration and Rate Constants for Cyanide Binding Determined by Stopped Flow

KatG	K_D (μM)[a]	k_{on} (M^{-1} s^{-1})[b]
wild-type	1.4 ± 0.2	4.4×10^5
Q293A	1.5 ± 0.2	4.8×10^5
IEEQ-A	19.3 ± 0.8	5.4×10^2
Δ291	9 ± 1	3.6×10^2
Δ291–292	17.5 ± 0.9	4.6×10^2
Δ290–293	43 ± 3	1.6×10^2
Δ288–293	23 ± 1	3.2×10^2
ΔLL2	21 ± 3	ND[c]

[a]All reactions conducted at 23 °C using 50 mM phosphate buffer (pH 7.0). [b]All reactions conducted at 25 °C using 50 mM phosphate buffer (pH 7.0). [c]Not determined.

Given the multiplicity of species evident in EPR spectra, we reasoned that the multiexponential nature of the cyanide binding progress curves may arise because of cyanide binding by distinct ferric species. For wild-type and Q293A KatG, the k_{obs} corresponding to the most rapid component of cyanide binding traces showed a linear dependence on cyanide concentration. From these data, second-order rate constants of 4.4×10^5 and 4.8×10^5 M^{-1} s^{-1} were obtained for wild-type and Q293A KatG, respectively. The former is in good agreement with second-order rate constants obtained for cyanide binding by KatGs from a variety of species.[26,52,66,67] The k_{obs} values corresponding to the second exponential of cyanide binding were ∼1 order of magnitude lower than those corresponding to the first. Similarly, the k_{obs} values corresponding to the third and fourth exponentials of these traces were 2 orders of magnitude and 500-fold lower than those corresponding to the first exponential, respectively.

For all the group II and III variants evaluated, the two most rapid exponentials observed with the wild-type and Q293A KatG appeared to be absent (Figure 5C,D). Indeed, subtraction of ΔA_{428} traces recorded for group II and III variants from those obtained for the wild type left a residual two-exponential function (Figure 5D), the k_{obs} values of which correspond to the two most rapid phases of cyanide binding by the wild-type enzyme. The most rapid component of cyanide binding by group II and III variants was linearly dependent on cyanide concentration, yielding second-order k_{on} values ranging between 1.6×10^2 and 5.4×10^2 M^{-1} s^{-1} (Table 5). Interestingly, there was also a marked difference in estimated k_{off} values when comparing the most rapid exponential of cyanide binding by wild-type and Q293A KatG (∼10 s^{-1}) to the most rapid exponential of cyanide binding by the group II and III variants (∼0.2 s^{-1}). This explained why the increase in the apparent K_D was considerably smaller than the decrease in the k_{on} observed for group II and III variants compared to that of the wild-type enzyme.

The effect of cyanide concentration on formation of the Fe^{III}–CN complex for the Δ288–293 variant (Figure 6) was typical of the group II and III variants. In addition to increased biexponential rates of complex formation, the amplitudes of

DOI: 10.1021/bi501221a
Biochemistry 2015, 54, 1648–1662

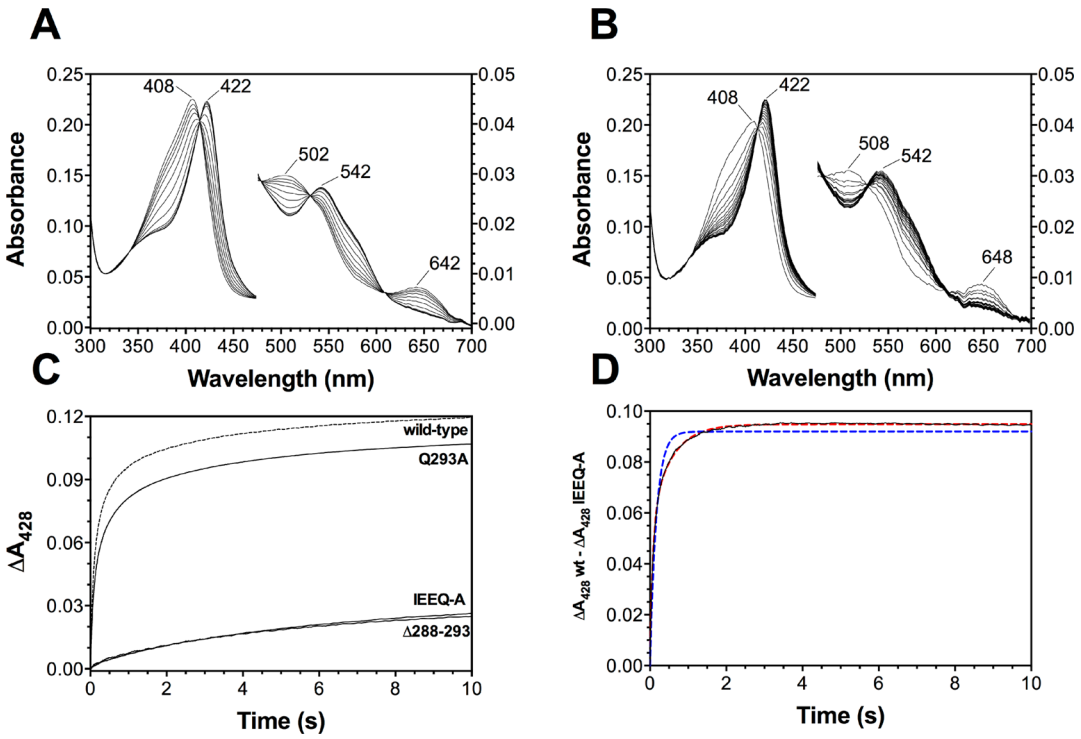

Figure 5. Kinetics of cyanide binding by KatG LL2 variants. Spectra recorded during reaction of (A) Q293A KatG with 0.015 mM cyanide (0.0189−18.9 s) and (B) IEEQ-A KatG with 0.5 mM cyanide (0.191−19.1 s) are shown. (C) Single-wavelength reaction traces (428 nm) for reaction of wild-type KatG, the group I variant representative Q293A, the group II variant representative IEEQ-A, and the group III variant representative Δ288−293 KatG with 0.015 mM cyanide are shown. (D) The ΔA_{428} values recorded for IEEQ-A during its reaction with 0.015 mM cyanide were subtracted from ΔA_{428} values recorded for the wild type under the same conditions. The resulting curve was fit to a single-exponential function (blue dashed line; k_{obs} = 5.99 s^{-1}) and a double-exponential function (red dashed line; k_{obs1} = 13.5 s^{-1}, and k_{obs2} = 1.87 s^{-1}). The k_{obs} values used to fit the original trace obtained from the wild-type reaction with 0.015 mM KCN were as follows: k_{obs1} = 15.3 s^{-1}, k_{obs2} = 2.6 s^{-1}, k_{obs3} = 0.29 s^{-1}, and k_{obs4} = 0.03 s^{-1}. Those obtained for IEEQ-A under the same conditions were as follows: k_{obs1} = 0.30 s^{-1}, and k_{obs2} = 0.04 s^{-1}. All reaction mixtures contained 3 μM protein and all reactions conducted at 25 °C using 50 mM phosphate buffer (pH 7.0).

each exponential showed a hyperbolic increase with cyanide concentration as did their sum (Figure 6B). Each curve was described well by a single K_D, and these values were similar to one another, with that determined for the sum falling between those obtained for the individual components (Table 6).

DISCUSSION

To date, only two variants targeting the LL2 structure of KatG have been reported. The absence of the structure in its entirety has been shown to eliminate catalase activity[50] as does a W300G substitution in *M. tuberculosis* KatG.[49] However, both variants retain some, albeit limited, peroxidatic function. Our data shed light on the role and importance of LL2, particularly its length, in KatG catalytic function. A series of substitution variants targeting the apex of LL2 had a minimal impact on the catalytic ability (catalase or peroxidase) of KatG. Similarly, the structure of the active site of these variants as determined by MCD and EPR spectroscopies was typically very similar to that of the wild-type enzyme. Hints of disruption were observed with Q293E KatG and I290A/Q293A KatG where EPR spectra were indicative of altered active sites. However, this was not corroborated by MCD measurements, and the catalytic activity of these variants was impacted to a limited extent compared to that of wild-type KatG. We have previously observed very similar spectroscopic and catalytic behavior in R691A KatG.[28] This arginine forms a hydrogen bond with the backbone carbonyl oxygen of amino acid 293.[22]

In contrast, a marked effect on catalase activity was observed when all four residues at the LL2 apex were each replaced with alanine (i.e., IEEQ-A KatG). Further, deletion of only one residue at the LL2 apex (Δ291) was sufficient to produce a KatG with catalytic and spectroscopic properties nearly identical to those of IEEQ-A KatG. Deletion of two residues at the LL2 apex (i.e., Δ291−292) was sufficient to completely eliminate catalase activity. The same result was observed with deletion of four amino acids (i.e., Δ290−293), six amino acids (i.e., Δ288−293), or the entire LL2 structure (i.e., ΔLL2). Indeed, there was little if any difference between these group III variants in catalatic or peroxidatic activity, spectroscopic properties, or cyanide binding characteristics. Losing two residues at the LL2 apex produced the same result as losing the entire structure. Losing one residue was nearly as detrimental regardless of whether this was accomplished by removing the apical amino acid (E291) or by shortening the ascending and descending limbs of the LL2 structure by one amino acid each (ΔP285/ΔG294 or ΔN280/ΔS299). Indeed, it did not seem to matter whether the residues removed from the ascending and descending limbs of the LL2 structure were conserved (as in ΔP285/ΔG294) or not (as in ΔN280/ΔS299).

A striking feature of LL2 is the interaction of its apex with another KatG-unique structure, the C-terminal domain. This point of contact lies some 30 Å from the active site and appears to be dominated by relatively nonspecific van der Waals interactions. Nevertheless, to achieve the interaction requires

DOI: 10.1021/bi501221a
Biochemistry 2015, 54, 1648−1662

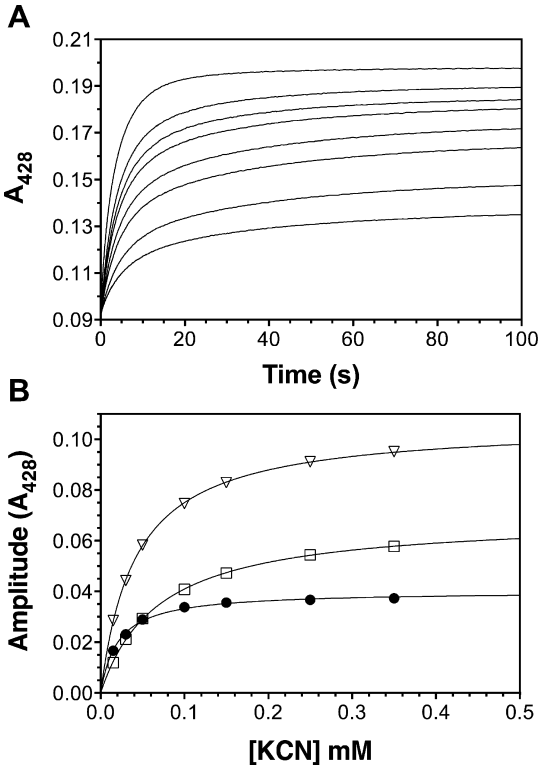

Figure 6. Effect of cyanide concentration on the extent of cyanide binding by Δ288−293 KatG. The effect of 0.015, 0.03, 0.05, 0.1, 0.15, 0.25, 0.35, and 0.5 mM cyanide on Δ288−293 KatG Fe^{III}−CN complex formation as monitored at 428 nm is shown in panel A. Reaction traces were fit to a two-exponential function. The effects of cyanide concentration on the pre-exponential factors (i.e., amplitudes) are shown in panel B. The amplitude corresponding to the more rapid of the two exponentials (□), the amplitude corresponding to the slower of the two exponentials (●), and the sum of the two amplitudes (▽) are all shown. All reaction mixtures contained 3 μM enzyme and all reactions conducted at 25 °C using 50 mM phosphate buffer (pH 7.0).

the LL2 polypeptide to traverse from its origin near the entrance to the active site to its point of contact with the C-terminal domain and back to its termination near its point of origin. This arrangement and the essentially invariant length of LL2 across all KatGs implies a length requirement to achieve an important interaction. Our data support this hypothesis.

The catalytic, spectroscopic, and ligand binding properties of IEEQ-A and all the deletion variants indicate that LL2 may be necessary to support an arrangement of active site H_2O molecules for efficient compound I formation. The peroxidase activity of all group II and III variants showed a dramatically diminished k_{cat}/K_M with respect to H_2O_2 and *tert*-butyl-OOH. Simultaneously, the k_{cat}/K_M with respect to the electron donor was equal to if not in excess of that observed for the wild-type enzyme. Together, these data suggested that oxidation of the ferric enzyme to compound I was compromised in the group II and III variants, but compound I reduction by peroxidatic electron donors was not. The k_{on} values for cyanide binding were diminished by 3 orders of magnitude for these same variants, verifying the diminished reactivity of the ferric state.

Without exception, MCD and EPR spectra for IEEQ-A KatG and all the deletion variants indicated shifts in the active site arrangement compared to that of the wild-type enzyme. In particular, EPR data suggest a shift in the position of H_2O molecules on the distal side of the heme. Other KatG variants have shown a diminished capacity to react with peroxide to form compound I or react with cyanide to form the Fe^{III}−CN complex because of the inclusion of a strong-field sixth ligand (e.g., the distal histidine) to the coordination sphere of the heme iron.[26−28,62] However, the virtual absence of hexacoordinate low-spin species in MCD and EPR spectra argued against this possibility with these variants. Rather, we observed a marked shift in the distribution of high-spin states. A typical feature of KatGs is a multiplicity of high-spin states present in the resting enzyme.[63,68,69] These states are distinguished by the degree of rhombic distortion observed for each one by EPR, and this has been taken to reflect the positioning of water molecules within the active site and, more generally, the state of the active site's hydrogen-bonded network.[63,65,70,71] Accordingly, previous reports have taken the species with the greatest extent of rhombic distortion ($g_x \sim 6.6$, $g_y \sim 4.95$, and $g_z \sim 1.95$) to be a pentacoordinate high-spin state where water is essentially absent from the coordination sphere of the heme iron. In contrast, lesser degrees of rhombic distortion are taken to reflect states where water is progressively and more ideally occupying the sixth coordination site of the iron.[63] Strikingly, for IEEQ-A KatG and all the deletion variants targeting LL2, the putative pentacoordinate state was much more prominent than in the wild type. Similarly, a purely axial state ($g_\perp \sim 5.85$, and $g_\parallel \sim 1.99$) where H_2O is thought to be a formal ligand to the heme iron clearly made a greater contribution to spectra for IEEQ-A and all the deletion variants than to the wild type, though it appeared to be a relatively small contributor in any case. In contrast, a narrow rhombic signal ($g_x \sim 6.0$, $g_y \sim 5.6$, and $g_z \sim 1.99$) where H_2O would occupy an intermediate position relative to the iron was an obvious contributor to the wild-type spectrum but virtually absent from those of IEEQ-A and all the deletion variants.

Table 6. Apparent K_D and Maximal Amplitudes from Kinetic Analysis of Cyanide Binding by Group II and III LL2 Variants

	exponential 1[a]			exponential 2[b]			total[c]	
KatG	K_D (μM)	amp. 1_{max}	%	K_D (μM)	amp. 2_{max}	%	K_D (μM)	amp_{max}
IEEQ-A	49	0.068	59	29	0.047	41	39	0.114
Δ291	57	0.069	62	10	0.042	38	28	0.106
Δ291−292	68	0.068	64	17	0.039	36	36	0.103
Δ290−293	380	0.086	65	31	0.046	35	78	0.099
Δ288−293	69	0.069	63	21	0.040	37	41	0.106
ΔLL2	88	0.081	69	24	0.037	31	53	0.132

[a]Amplitude analyses corresponding to the exponential function with the larger of two k_{obs} values. [b]Amplitude analyses corresponding to the exponential function with the smaller of two k_{obs} values. [c]Amplitude analyses corresponding to the sum of both exponentials.

DOI: 10.1021/bi501221a
Biochemistry 2015, 54, 1648−1662

We propose that a shift in the arrangement of active site water molecules suggested by the EPR and MCD spectra for IEEQ-A and the various LL2 deletion variants was also manifested in the diminished capacity of these proteins to react with peroxides (H_2O_2 and *tert*-butyl-OOH), presumably to form compound I (i.e., Fe^{IV}=O[porphyrin]$^{\bullet+}$), and to bind cyanide to form the Fe^{III}−CN complex. With respect to the latter, the most rapid phases of Fe^{III}−CN complex formation seen with wild-type KatG were absent from all group II and III variants evaluated. Precedent for the connection between active site water arrangement and cyanide binding in particular has been observed with KatG from *M. tuberculosis* and its isoniazid resistance variant S315T.[67] Using the effect of enzyme aging and amino acid substitution at position 315, rapid cyanide binding was assigned by EPR to a species with narrow rhombic distortion ($g_x \sim 5.94$, and $g_y \sim 5.49$). Similarly, cyanide binding rates diminished by 3 orders of magnitude were assigned to a species with greater **g** tensor anisotropy ($g_x \sim 6.33$, and $g_y \sim 5.09$). Cyanide binding by wild-type and S315T KatG was observed to be multiphasic, but the rate curves obtained for the S315T variant showed a contribution of slow cyanide binding greater than that detected with the wild type, consistent with the larger contribution of pentacoordinate states in the former compared to the latter. Accordingly, structures determined for the S315T MtKatG and the analogous S324T BpKatG (but not their wild-type counterparts) have shown water displaced from the coordination sphere of the heme iron.[72,73] Notably, this serine (S312 in *E. coli*) is immediately adjacent to the C-terminal end of LL2.

It has become increasingly clear that the distribution and/or arrangement of active site water molecules plays an important role in the reactivity and catalytic function of KatG and other heme proteins. For example, a critical event in the classical Poulos−Kraut mechanism for formation of compound I is the formation of compound 0, an Fe^{III}−OOH species. This requires the transfer of H^+ from the substrate H_2O_2 to the active site's general base, the distal histidine.[74] However, the distance between the distal histidine and the heme iron-bound peroxide imposes a kinetic barrier to proton transfer that contradicts the experimentally observed rates for compound 0 formation. Further, structures of enzymes from across the non-animal peroxidase superfamily are relatively rigid, suggesting that the distance is not closed by protein dynamic fluctuation.[75] Recent computational studies of horseradish peroxidase have shown that an intervening H_2O molecule could facilitate H^+ transfer and account for experimentally observed rates of compound 0 formation.[76] The shared active site structural features across the superfamily suggest that the same principle operates in KatG and other non-animal peroxidases.[75]

The utility of cyanide binding as a mimic of compound I formation arises from its similarity to formation of compound 0 by peroxide. With a pK_a above 9, HCN is the dominant species in formation of the Fe^{III}−CN complex, so transfer of H^+ to the protein, apparently to the distal histidine, accompanies this event.[19,64,77−81] An extensive evaluation of cyanide binding by metmyoglobin suggests an appropriately placed H_2O in the active site appears to facilitate the H^+ transfers necessary for cyanide binding.[82] Our studies with LL2 variants confirm that pentacoordinate high-spin species of KatG are uniformly slow in cyanide binding. However, our studies also seem to indicate that true axial hexacoordinate high-spin species are also slow in this respect, perhaps because the H_2O ligand must be displaced prior to Fe^{III}−CN complex formation. A structure in which H_2O occupies an intermediate position may be optimal. Thus far, the greatest cyanide binding and catalytic activity of KatG appear to correlate with a species showing narrow rhombic distortion by EPR. It is interesting to note that both k_{on} and k_{off} for the Fe^{III}−CN complex were dramatically diminished with the group II and III LL2 variants of KatG. This makes sense if an active site H_2O acts as a H^+ relay. Presumably, the reverse reaction (i.e., dissociation of a CN group from the heme) would be facilitated by protonation to re-form HCN.

In both its structure and function, LL2 stands in contrast to the other prominent extended loop structure in KatGs, LL1. Where LL2 tolerates little if any adjustment in its length, a substantial portion of LL1 (amino acids 200−214) has been eliminated by deletion mutagenesis, and the catalytic properties of the variant are virtually indistinguishable from those of the wild-type enzyme.[36] Further, though deletion of another section of LL1 (Δ209−228) or the entire structure (ΔLL1) does eliminate catalase activity, this is largely due to the absence of Y226, the strictly conserved tyrosine that participates in the MYW covalent adduct of the enzyme. Indeed, even without residues 209−228, the peroxidase activity of KatG was enhanced by a factor of 10. In nearly all instances where deletions or substitutions of LL1 amino acids result in the loss of catalytic function are made, it is not compound I formation but rather the *catalatic* reduction of compound I that is diminished or eliminated.

Interestingly, the results of studies on both structures comport with the nature of conservation as it is observed across KatGs. The LL1 structure varies substantially in length, but its C-terminal end shows little variability in sequence across all KatGs. In contrast, LL2 is virtually invariant in its length, and though strictly conserved amino acids are observed in the structure, almost all of them are either proline or glycine, both of which are known for their unique impact on polypeptide conformation and dynamics. Outside of proline and glycine, W297 (W300 in MtKatG) is one residue that appears to be strictly conserved across KatGs. Variants targeting this residue provide an interesting corroboration of our results. Replacement of this tryptophan with glycine, a residue that allows exploration of a much wider range of conformations (i.e., W300G MtKatG), produces a protein with catalytic properties that appear to be similar to those of our group III variants.[49] However, a substitution that does not appreciably change the conformational flexibility of LL2 (i.e., our W297F *E. coli* KatG variant) has catalytic properties indistinguishable from those of the wild-type enzyme.

■ ASSOCIATED CONTENT

Supporting Information

Primer sequences used to generate the variants evaluated in this study, the background for steady-state evaluation of peroxidase reaction kinetics, an SDS−PAGE gel to evaluate the formation of the MYW adduct in wild-type and ΔLL2 KatG, and spectra corresponding to equilibrium titrations with cyanide for wild-type, Q293A, IEEQ-A, and Δ288−293 KatG. This material is available free of charge via the Internet at http://pubs.acs.org.

■ AUTHOR INFORMATION

Corresponding Author

*E-mail: goodwdc@auburn.edu. Phone: (334) 844-6992. Fax: (334) 844-6959.

DOI: 10.1021/bi501221a
Biochemistry 2015, 54, 1648−1662

Present Addresses

[†]S.N.K.: Department of Biochemistry, Vanderbilt University School of Medicine, Nashville, TN 37205-0146.

[‡]Y.L.: Department of Molecular and Experimental Medicine, The Scripps Research Institute, La Jolla, CA 92037.

Funding

This work was supported in part by National Science Foundation Grant MCB0641614.

Notes

The authors declare no competing financial interest.

■ ACKNOWLEDGMENTS

We thank Dr. Steve Mansoorabadi and his group for access to the Agilent 1260 Infinity HPLC instrument for size-exclusion studies, Dr. Angela Calderón for access to the Agilent 6520 Q-TOF instrument, and Dr. Holly Ellis and Dr. Johayra Simithy for helpful discussions. We also thank Eric Bowman and the staff at Davis Sequencing, Inc., for rapid and reliable service in the substantial DNA sequence analyses required for this work.

■ ABBREVIATIONS

KatG, catalase-peroxidase; MtKatG, *M. tuberculosis* KatG; BpKatG, *Bu. pseudomallei* KatG; LL1, large loop 1; LL2, large loop 2; LL3, large loop 3; MYW, methionine-tyrosine-tryptophan covalent adduct; IPTG, isopropyl β-D-thiogalacto-pyranoside; Ni-NTA, nickel-nitriloacetic acid; ABTS, 2,2′-azinobis(3-ethylbenzthiazoline-6-sulfonic acid); MCD, magnetic circular dichroism.

■ REFERENCES

(1) Zamocky, M., Furtmuller, P. G., and Obinger, C. (2010) Evolution of structure and function of class I peroxidases. *Arch. Biochem. Biophys. 500*, 45−57.

(2) Njuma, O. J., Ndontsa, E. N., and Goodwin, D. C. (2014) Catalase in peroxidase clothing: Interdependent cooperation of two cofactors in the catalytic versatility of KatG. *Arch. Biochem. Biophys. 544*, 27−39.

(3) Uhlich, G. A. (2009) KatP contributes to OxyR-regulated hydrogen peroxide resistance in *Escherichia coli* serotype O157: H7. *Microbiology 155*, 3589−3598.

(4) Brunder, W., Schmidt, H., and Karch, H. (1996) KatP, a novel catalase-peroxidase encoded by the large plasmid of enterohaemorrhagic *Escherichia coli* O157:H7. *Microbiology 142*, 3305−3315.

(5) Bandyopadhyay, P., Byrne, B., Chan, Y., Swanson, M. S., and Steinman, H. M. (2003) *Legionella pneumophila* catalase-peroxidases are required for proper trafficking and growth in primary macrophages. *Infect. Immun. 71*, 4526−4535.

(6) Garcia, E., Nedialkov, Y. A., Elliott, J., Motin, V. L., and Brubaker, R. R. (1999) Molecular characterization of KatY (antigen 5), a thermoregulated chromosomally encoded catalase-peroxidase of *Yersinia pestis*. *J. Bacteriol. 181*, 3114−3122.

(7) Mehigh, R. J., and Brubaker, R. R. (1993) Major stable peptides of *Yersinia pestis* synthesized during the low-calcium response. *Infect. Immun. 61*, 13−22.

(8) Zamocky, M., Droghetti, E., Bellei, M., Gasselhuber, B., Pabst, M., Furtmuller, P. G., Battistuzzi, G., Smulevich, G., and Obinger, C. (2012) Eukaryotic extracellular catalase-peroxidase from *Magnaporthe grisea*: Biophysical/chemical characterization of the first representative from a novel phytopathogenic KatG group. *Biochimie 94*, 673−683.

(9) Zamocky, M., Furtmuller, P. G., Bellei, M., Battistuzzi, G., Stadlmann, J., Vlasits, J., and Obinger, C. (2009) Intracellular catalase/peroxidase from the phytopathogenic rice blast fungus *Magnaporthe grisea*: Expression analysis and biochemical characterization of the recombinant protein. *Biochem. J. 418*, 443−451.

(10) Zamocky, M., Furtmuller, P. G., and Obinger, C. (2009) Two distinct groups of fungal catalase/peroxidases. *Biochem. Soc. Trans. 37*, 772−777.

(11) Tanabe, S., Ishii-Minami, N., Saitoh, K., Otake, Y., Kaku, H., Shibuya, N., Nishizawa, Y., and Minami, E. (2011) The role of catalase-peroxidase secreted by *Magnaporthe oryzae* during early infection of rice cells. *Mol. Plant-Microbe Interact. 24*, 163−171.

(12) Singh, R., Wiseman, B., Deemagarn, T., Jha, V., Switala, J., and Loewen, P. C. (2008) Comparative study of catalase-peroxidases (KatGs). *Arch. Biochem. Biophys. 471*, 207−214.

(13) Switala, J., and Loewen, P. C. (2002) Diversity of properties among catalases. *Arch. Biochem. Biophys. 401*, 145−154.

(14) Zamocky, M., Gasselhuber, B., Furtmuller, P. G., and Obinger, C. (2014) Turning points in the evolution of peroxidase-catalase superfamily: Molecular phylogeny of hybrid heme peroxidases. *Cell. Mol. Life Sci. 71*, 4681−4696.

(15) Jasion, V. S., Polanco, J. A., Meharenna, Y. T., Li, H., and Poulos, T. L. (2011) Crystal structure of *Leishmania major* peroxidase and characterization of the compound I tryptophan radical. *J. Biol. Chem. 286*, 24608−24615.

(16) Finzel, B. C., Poulos, T. L., and Kraut, J. (1984) Crystal structure of yeast cytochrome *c* peroxidase refined at 1.7-Å resolution. *J. Biol. Chem. 259*, 13027−13036.

(17) Patterson, W. R., and Poulos, T. L. (1995) Crystal structure of recombinant pea cytosolic ascorbate peroxidase. *Biochemistry 34*, 4331−4341.

(18) Yamada, Y., Fujiwara, T., Sato, T., Igarashi, N., and Tanaka, N. (2002) The 2.0 angstrom crystal structure of catalase-peroxidase from *Haloarcula marismortui*. *Nat. Struct. Biol. 9*, 691−695.

(19) Dunford, H. B. (1999) *Heme Peroxidases*, Wiley-VCH, New York.

(20) Sivaraja, M., Goodin, D. B., Smith, M., and Hoffman, B. M. (1989) Identification by ENDOR of Trp191 as the free-radical site in cytochrome-*c* peroxidase compound ES. *Science 245*, 738−740.

(21) Ivancich, A., Dorlet, P., Goodin, D. B., and Un, S. (2001) Multifrequency high-field EPR study of the tryptophanyl and tyrosyl radical intermediates in wild-type and the W191G mutant of cytochrome *c* peroxidase. *J. Am. Chem. Soc. 123*, 5050−5058.

(22) Carpena, X., Loprasert, S., Mongkolsuk, S., Switala, J., Loewen, P. C., and Fita, I. (2003) Catalase-peroxidase KatG of *Burkholderia pseudomallei* at 1.7 Å resolution. *J. Mol. Biol. 327*, 475−489.

(23) Bertrand, T., Eady, N. A. J., Jones, J. N., Nagy, J. M., Jamart-Gregoire, B., Raven, E. L., and Brown, K. A. (2004) Crystal structure of *Mycobacterium tuberculosis* catalase-peroxidase. *J. Biol. Chem. 279*, 38991−38999.

(24) Welinder, K. G. (1991) Bacterial catalase-peroxidases are gene duplicated members of the plant peroxidase superfamily. *Biochim. Biophys. Acta 1080*, 215−220.

(25) Zamocky, M., Regelsberger, G., Jakopitsch, C., and Obinger, C. (2001) The molecular peculiarities of catalase-peroxidases. *FEBS Lett. 492*, 177−182.

(26) Baker, R. D., Cook, C. O., and Goodwin, D. C. (2004) Properties of catalase-peroxidase lacking its C-terminal domain. *Biochem. Biophys. Res. Commun. 320*, 833−839.

(27) Baker, R. D., Cook, C. O., and Goodwin, D. C. (2006) Catalase-peroxidase active site restructuring by a distant and "inactive" domain. *Biochemistry 45*, 7113−7121.

(28) Wang, Y., and Goodwin, D. C. (2013) Integral role of the I′-helix in the function of the "inactive" C-terminal domain of catalase-peroxidase (KatG). *Biochim. Biophys. Acta 1834*, 362−371.

(29) Zamocky, M., Garcia-Fernandez, Q., Gasselhuber, B., Jakopitsch, C., Furtmuller, P. G., Loewen, P. C., Fita, I., Obinger, C., and Carpena, X. (2012) High conformational stability of secreted eukaryotic catalase-peroxidases: Answers from first crystal structure and unfolding studies. *J. Biol. Chem. 287*, 32254−32262.

(30) Donald, L. J., Krokhin, O. V., Duckworth, H. W., Wiseman, B., Deemagarn, T., Singh, R., Switala, J., Carpena, X., Fita, I., and Loewen, P. C. (2003) Characterization of the catalase-peroxidase KatG from

DOI: 10.1021/bi501221a
Biochemistry 2015, 54, 1648−1662

Burkholderia pseudomallei by mass spectrometry. *J. Biol. Chem. 278*, 35687−35692.
(31) Jakopitsch, C., Kolarich, D., Petutschnig, G., Furtmuller, P. G., and Obinger, C. (2003) Distal side tryptophan, tyrosine and methionine in catalase-peroxidases are covalently linked in solution. *FEBS Lett. 552*, 135−140.
(32) Ghiladi, R. A., Knudsen, G. M., Medzihradszky, K. F., and Ortiz de Montellano, P. R. (2005) The Met-Tyr-Trp cross-link in *Mycobacterium tuberculosis* catalase-peroxidase (KatG): Autocatalytic formation and effect on enzyme catalysis and spectroscopic properties. *J. Biol. Chem. 280*, 22651−22663.
(33) Ghiladi, R. A., Medzihradszky, K. F., and Ortiz de Montellano, P. R. (2005) Role of the Met-Tyr-Trp cross-link in *Mycobacterium tuberculosis* catalase-peroxidase (KatG) as revealed by KatG(M255I). *Biochemistry 44*, 15093−15105.
(34) Regelsberger, G., Jakopitsch, C., Furtmuller, P. G., Rueker, F., Switala, J., Loewen, P. C., and Obinger, C. (2001) The role of distal tryptophan in the bifunctional activity of catalase-peroxidases. *Biochem. Soc. Trans. 29*, 99−105.
(35) Regelsberger, G., Jakopitsch, C., Ruker, F., Krois, D., Peschek, G. A., and Obinger, C. (2000) Effect of distal cavity mutations on the formation of compound I in catalase-peroxidases. *J. Biol. Chem. 275*, 22854−22861.
(36) Kudalkar, S. N., Campbell, R. A., Li, Y., Varnado, C. L., Prescott, C., and Goodwin, D. C. (2012) Enhancing the peroxidatic activity of KatG by deletion mutagenesis. *J. Inorg. Biochem. 116C*, 106−115.
(37) Yu, S. W., Girotto, S., Zhao, X. B., and Magliozzo, R. S. (2003) Rapid formation of Compound II and a tyrosyl radical in the Y229F mutant of *Mycobacterium tuberculosis* catalase-peroxidase disrupts catalase but not peroxidase function. *J. Biol. Chem. 278*, 44121−44127.
(38) Hillar, A., Peters, B., Pauls, R., Loboda, A., Zhang, H., Mauk, A. G., and Loewen, P. C. (2000) Modulation of the activities of catalase-peroxidase HPI of *Escherichia coli* by site-directed mutagenesis. *Biochemistry 39*, 5868−5875.
(39) Jakopitsch, C., Auer, M., Ivancich, A., Ruker, F., Furtmuller, P. G., and Obinger, C. (2003) Total conversion of bifunctional catalase-peroxidase (KatG) to monofunctional peroxidase by exchange of a conserved distal side tyrosine. *J. Biol. Chem. 278*, 20185−20191.
(40) Loewen, P. C., Carpena, X., Vidossich, P., Fita, I., and Rovira, C. (2014) An ionizable active-site tryptophan imparts catalase activity to a peroxidase core. *J. Am. Chem. Soc. 136*, 7249−7252.
(41) Suarez, J., Ranguelova, K., Jarzecki, A. A., Manzerova, J., Krymov, V., Zhao, X., Yu, S., Metlitsky, L., Gerfen, G. J., and Magliozzo, R. S. (2009) An oxyferrous heme/protein-based radical intermediate is catalytically competent in the catalase reaction of *Mycobacterium tuberculosis* catalase-peroxidase (KatG). *J. Biol. Chem. 284*, 7017−7029.
(42) Zhao, X., Khajo, A., Jarrett, S., Suarez, J., Levitsky, Y., Burger, R. M., Jarzecki, A. A., and Magliozzo, R. S. (2012) Specific function of the Met-Tyr-Trp adduct radical and residues Arg-418 and Asp-137 in the atypical catalase reaction of catalase-peroxidase KatG. *J. Biol. Chem. 287*, 37057−37065.
(43) Zhao, X., Suarez, J., Khajo, A., Yu, S., Metlitsky, L., and Magliozzo, R. S. (2010) A radical on the Met-Tyr-Trp modification required for catalase activity in catalase-peroxidase is established by isotopic labeling and site-directed mutagenesis. *J. Am. Chem. Soc. 132*, 8268−8269.
(44) Vlasits, J., Jakopitsch, C., Bernroitner, M., Zamocky, M., Furtmuller, P. G., and Obinger, C. (2010) Mechanisms of catalase activity of heme peroxidases. *Arch. Biochem. Biophys. 500*, 74−81.
(45) Jakopitsch, C., Wanasinghe, A., Jantschko, W., Furtmuller, P. G., and Obinger, C. (2005) Kinetics of interconversion of ferrous enzymes, compound II and compound III, of wild-type *Synechocystis* catalase-peroxidase and Y249F: Proposal for the catalatic mechanism. *J. Biol. Chem. 280*, 9037−9042.
(46) Jakopitsch, C., Droghetti, E., Schmuckenschlager, F., Furtmuller, P. G., Smulevich, G., and Obinger, C. (2005) Role of the main access channel of catalase-peroxidase in catalysis. *J. Biol. Chem. 280*, 42411−42422.
(47) Vlasits, J., Bellei, M., Jakopitsch, C., De Rienzo, F., Furtmuller, P. G., Zamocky, M., Sola, M., Battistuzzi, G., and Obinger, C. (2010) Disruption of the H-bond network in the main access channel of catalase-peroxidase modulates enthalpy and entropy of Fe(III) reduction. *J. Inorg. Biochem. 104*, 648−656.
(48) Zamocky, M., Garcia-Fernandez, Q., Gasselhuber, B., Jakopitsch, C., Furtmuller, P. G., Loewen, P. C., Fita, I., Obinger, C., and Carpena, X. (2012) High conformational stability of secreted eukaryotic catalase-peroxidases: Answers from first crystal structure and unfolding studies. *J. Biol. Chem. 287*, 32254−32262.
(49) Cade, C. E., Dlouhy, A. C., Medzihradszky, K. F., Salas-Castillo, S. P., and Ghiladi, R. A. (2010) Isoniazid-resistance conferring mutations in *Mycobacterium tuberculosis* KatG: Catalase, peroxidase, and INH-NADH adduct formation activities. *Protein Sci. 19*, 458−474.
(50) Li, Y., and Goodwin, D. C. (2004) Vital roles of an interhelical insertion in catalase-peroxidase bifunctionality. *Biochem. Biophys. Res. Commun. 318*, 970−976.
(51) Moore, S. 'Round-the-horn site-directed mutagenesis. OpenWetWare http://openwetware.org/wiki/'Round-the-horn_site-directed_mutagenesis (accessed June 2014).
(52) Varnado, C. L., Hertwig, K. M., Thomas, R., Roberts, J. K., and Goodwin, D. C. (2004) Properties of a novel periplasmic catalase-peroxidase from *Escherichia coli* O157:H7. *Arch. Biochem. Biophys. 421*, 166−174.
(53) Gill, S. C., and von Hippel, P. H. (1989) Calculation of protein extinction coefficients from amino acid sequence data. *Anal. Biochem. 182*, 319−326.
(54) Falk, J. K. (1964) in *Porphyrins and Metalloporphyrins* (Smith, K. M., Ed.) pp 804−807, Elsevier Publishing, New York.
(55) Hagen, W. R. (2009) *Biomolecular EPR spectroscopy*, CRC Press, Boca Raton, FL.
(56) Hagen, W. R. (2012) TU Delft: Biomolecular EPR Spectroscopy. http://www.bt.tudelft.nl/biomolecularEPRspectroscopy.
(57) Nelson, D. P., and Kiesow, L. A. (1972) Enthalpy of decomposition of hydrogen peroxide by catalase at 25 °C (with molar extinction coefficients of H_2O_2 solutions in UV). *Anal. Biochem. 49*, 474−478.
(58) Scott, S. L., Chen, W. J., Bakac, A., and Espenson, J. H. (1993) Spectroscopic parameters, electrode-potentials, acid ionization-constants, and electron-exchange rates of the 2,2′-azinobis(3-ethylbenzothiazoline-6-sulfonate) radicals and ions. *J. Phys. Chem. 97*, 6710−6714.
(59) Claiborne, A., and Fridovich, I. (1979) Purification of the o-dianisidine peroxidase from *Escherichia coli* B. Physicochemical characterization and analysis of its dual catalatic and peroxidatic activities. *J. Biol. Chem. 254*, 4245−4252.
(60) Cheesman, M. R., Greenwood, C., and Thomson, A. J. (1991) Magnetic circular dichroism of hemoproteins. *Adv. Inorg. Chem. 36*, 201−255.
(61) Cheek, J., Mandelman, D., Poulos, T. L., and Dawson, J. H. (1999) A study of the K^+-site mutant of ascorbate peroxidase: Mutations of protein residues on the proximal side of the heme cause changes in iron ligation on the distal side. *JBIC, J. Biol. Inorg. Chem. 4*, 64−72.
(62) Moore, R. L., Cook, C. O., Williams, R., and Goodwin, D. C. (2008) Substitution of strictly conserved Y111 in catalase-peroxidases: Impact of remote interdomain contacts on active site structure and catalytic performance. *J. Inorg. Biochem. 102*, 1819−1824.
(63) Svistunenko, D. A., Worrall, J. A., Chugh, S. B., Haigh, S. C., Ghiladi, R. A., and Nicholls, P. (2012) Ferric haem forms of *Mycobacterium tuberculosis* catalase-peroxidase probed by EPR spectroscopy: Their stability and interplay with pH. *Biochimie 94*, 1274−1280.
(64) Dunford, H. B., Hewson, W. D., and Steiner, H. (1978) Horseradish peroxidase. 29. Reactions in water and deuterium-oxide, cyanide binding, compound-I formation, and reactions of compound-I and compound-II with ferrocyanide. *Can. J. Chem. 56*, 2844−2852.
(65) Jakopitsch, C., Ivancich, A., Schmuckenschlager, F., Wanasinghe, A., Poltl, G., Furtmuller, P. G., Ruker, F., and Obinger, C. (2004)

DOI: 10.1021/bi501221a
Biochemistry 2015, 54, 1648−1662

Influence of the unusual covalent adduct on the kinetics and formation of radical intermediates in *Synechocystis* catalase peroxidase: A stopped-flow and EPR characterization of the Met275, Tyr249, and Arg439 variants. *J. Biol. Chem. 279*, 46082−46095.
(66) Jakopitsch, C., Ruker, F., Regelsberger, G., Dockal, M., Peschek, G. A., and Obinger, C. (1999) Catalase-peroxidase from the cyanobacterium *Synechocystis* PCC 6803: Cloning, overexpression in *Escherichia coli*, and kinetic characterization. *Biol. Chem. 380*, 1087−1096.
(67) Ranguelova, K., Suarez, J., Metlitsky, L., Yu, S., Brejt, S. Z., Zhao, L., Schelvis, J. P., and Magliozzo, R. S. (2008) Impact of distal side water and residue 315 on ligand binding to ferric *Mycobacterium tuberculosis* catalase-peroxidase (KatG). *Biochemistry 47*, 12583−12592.
(68) Wengenack, N. L., Todorovic, S., Yu, L., and Rusnak, F. (1998) Evidence for differential binding of isoniazid by *Mycobacterium tuberculosis* KatG and the isoniazid-resistant mutant KatG(S315T). *Biochemistry 37*, 15825−15834.
(69) Ivancich, A., Jakopitsch, C., Auer, M., Un, S., and Obinger, C. (2003) Protein-based radicals in the catalase-peroxidase of *Synechocystis* PCC6803: A multifrequency EPR investigation of wild-type and variants on the environment of the heme active site. *J. Am. Chem. Soc. 125*, 14093−14102.
(70) Colin, J., Jakopitsch, C., Obinger, C., and Ivancich, A. (2010) The Reaction of *Synechocystis* catalase-peroxidase (KatG) with isoniazid investigated by multifrequency (9−285 GHz) EPR spectroscopy. *Appl. Magn. Reson. 37*, 267−277.
(71) Jakopitsch, C., Obinger, C., Un, S., and Ivancich, A. (2006) Identification of Trp106 as the tryptophanyl radical intermediate in *Synechocystis* PCC6803 catalase-peroxidase by multifrequency electron paramagnetic resonance spectroscopy. *J. Inorg. Biochem. 100*, 1091−1099.
(72) Zhao, X., Yu, H., Yu, S., Wang, F., Sacchettini, J. C., and Magliozzo, R. S. (2006) Hydrogen peroxide-mediated isoniazid activation catalyzed by *Mycobacterium tuberculosis* catalase-peroxidase (KatG) and its S315T mutant. *Biochemistry 45*, 4131−4140.
(73) Deemagarn, T., Carpena, X., Singh, R., Wiseman, B., Fita, I., and Loewen, P. C. (2005) Structural characterization of the Ser324Thr variant of the catalase-peroxidase (KatG) from *Burkholderia pseudomallei*. *J. Mol. Biol. 345*, 21−28.
(74) Poulos, T. L., and Kraut, J. (1980) The stereochemistry of peroxidase catalysis. *J. Biol. Chem. 255*, 8199−8205.
(75) Vidossich, P., Alfonso-Prieto, M., Carpena, X., Fita, I., Loewen, P. C., and Rovira, C. (2010) The dynamic role of distal side residues in heme hydroperoxidase catalysis: Interplay between X-ray crystallography and *ab initio* MD simulations. *Arch. Biochem. Biophys. 500*, 37−44.
(76) Derat, E., Shaik, S., Rovira, C., Vidossich, P., and Alfonso-Prieto, M. (2007) The effect of a water molecule on the mechanism of formation of compound 0 in horseradish peroxidase. *J. Am. Chem. Soc. 129*, 6346−6347.
(77) Ellis, W. D., and Dunford, H. B. (1968) Kinetics of cyanide and fluoride binding by ferric horseradish peroxidase. *Biochemistry 7*, 2054−2062.
(78) Thanabal, V., Deropp, J. S., and Lamar, G. N. (1988) Proton NMR characterization of the catalytically relevant proximal and distal hydrogen-bonding networks in ligated resting state horseradish peroxidase. *J. Am. Chem. Soc. 110*, 3027−3035.
(79) Deropp, J. S., Lamar, G. N., Wariishi, H., and Gold, M. H. (1991) NMR-study of the active-site of resting state and cyanide-inhibited lignin peroxidase from *Phanerochaete chrysosporium*: Comparison with horseradish-peroxidase. *J. Biol. Chem. 266*, 15001−15008.
(80) Fukuyama, K., and Okada, T. (2007) Structures of cyanide, nitric oxide and hydroxylamine complexes of *Arthromyces ramosus* peroxidase at 100 K refined to 1.3 Å resolution: Coordination geometries of the ligands to the haem iron. *Acta Crystallogr. D63*, 472−477.
(81) Henriksen, A., Smith, A. T., and Gajhede, M. (1999) The structures of the horseradish peroxidase C-ferulic acid complex and the ternary complex with cyanide suggest how peroxidases oxidize small phenolic substrates. *J. Biol. Chem. 274*, 35005−35011.
(82) Brancaccio, A., Cutruzzola, F., Allocatelli, C. T., Brunori, M., Smerdon, S. J., Wilkinson, A. J., Dou, Y., Keenan, D., Ikeda-Saito, M., Brantley, R. E., Jr., and Olson, J. S. (1994) Structural factors governing azide and cyanide binding to mammalian metmyoglobins. *J. Biol. Chem. 269*, 13843−13853.
(83) *PyMOL Molecular Graphics System* (2013) Schrodinger, LLC, Portland, OR.

DOI: 10.1021/bi501221a
Biochemistry 2015, 54, 1648−1662